CLEO-CONF 05-4
LP2005-431

Measurement of Inclusive Production of η, η' and ϕ Mesons in D^o and D^+ Decays*

M. Artuso,[1] C. Boulahouache,[1] S. Blusk,[1] J. Butt,[1] O. Dorjkhaidav,[1] J. Li,[1] N. Menaa,[1] R. Mountain,[1] R. Nandakumar,[1] K. Randrianarivony,[1] R. Redjimi,[1] R. Sia,[1] T. Skwarnicki,[1] S. Stone,[1] J. C. Wang,[1] K. Zhang,[1] S. E. Csorna,[2] G. Bonvicini,[3] D. Cinabro,[3] M. Dubrovin,[3] R. A. Briere,[4] G. P. Chen,[4] J. Chen,[4] T. Ferguson,[4] G. Tatishvili,[4] H. Vogel,[4] M. E. Watkins,[4] J. L. Rosner,[5] N. E. Adam,[6] J. P. Alexander,[6] K. Berkelman,[6] D. G. Cassel,[6] V. Crede,[6] J. E. Duboscq,[6] K. M. Ecklund,[6] R. Ehrlich,[6] L. Fields,[6] L. Gibbons,[6] B. Gittelman,[6] R. Gray,[6] S. W. Gray,[6] D. L. Hartill,[6] B. K. Heltsley,[6] D. Hertz,[6] C. D. Jones,[6] J. Kandaswamy,[6] D. L. Kreinick,[6] V. E. Kuznetsov,[6] H. Mahlke-Krüger,[6] T. O. Meyer,[6] P. U. E. Onyisi,[6] J. R. Patterson,[6] D. Peterson,[6] E. A. Phillips,[6] J. Pivarski,[6] D. Riley,[6] A. Ryd,[6] A. J. Sadoff,[6] H. Schwarthoff,[6] X. Shi,[6] M. R. Shepherd,[6] S. Stroiney,[6] W. M. Sun,[6] D. Urner,[6] T. Wilksen,[6] K. M. Weaver,[6] M. Weinberger,[6] S. B. Athar,[7] P. Avery,[7] L. Breva-Newell,[7] R. Patel,[7] V. Potlia,[7] H. Stoeck,[7] J. Yelton,[7] P. Rubin,[8] C. Cawlfield,[9] B. I. Eisenstein,[9] G. D. Gollin,[9] I. Karliner,[9] D. Kim,[9] N. Lowrey,[9] P. Naik,[9] C. Sedlack,[9] M. Selen,[9] E. J. White,[9] J. Williams,[9] J. Wiss,[9] K. W. Edwards,[10] D. Besson,[11] T. K. Pedlar,[12] D. Cronin-Hennessy,[13] K. Y. Gao,[13] D. T. Gong,[13] J. Hietala,[13] Y. Kubota,[13] T. Klein,[13] B. W. Lang,[13] S. Z. Li,[13] R. Poling,[13] A. W. Scott,[13] A. Smith,[13] S. Dobbs,[14] Z. Metreveli,[14] K. K. Seth,[14] A. Tomaradze,[14] P. Zweber,[14] J. Ernst,[15] H. Severini,[16] D. M. Asner,[17] S. A. Dytman,[17] W. Love,[17] S. Mehrabyan,[17] J. A. Mueller,[17] V. Savinov,[17] Z. Li,[18] A. Lopez,[18] H. Mendez,[18] J. Ramirez,[18] G. S. Huang,[19] D. H. Miller,[19] V. Pavlunin,[19] B. Sanghi,[19] I. P. J. Shipsey,[19] G. S. Adams,[20] M. Cravey,[20] J. P. Cummings,[20] I. Danko,[20] J. Napolitano,[20] Q. He,[21] H. Muramatsu,[21] C. S. Park,[21] E. H. Thorndike,[21] T. E. Coan,[22] Y. S. Gao,[22] and F. Liu[22]

(CLEO Collaboration)

[1] *Syracuse University, Syracuse, New York 13244*
[2] *Vanderbilt University, Nashville, Tennessee 37235*
[3] *Wayne State University, Detroit, Michigan 48202*
[4] *Carnegie Mellon University, Pittsburgh, Pennsylvania 15213*
[5] *Enrico Fermi Institute, University of Chicago, Chicago, Illinois 60637*
[6] *Cornell University, Ithaca, New York 14853*
[7] *University of Florida, Gainesville, Florida 32611*
[8] *George Mason University, Fairfax, Virginia 22030*
[9] *University of Illinois, Urbana-Champaign, Illinois 61801*
[10] *Carleton University, Ottawa, Ontario, Canada K1S 5B6 and the Institute of Particle Physics, Canada*
[11] *University of Kansas, Lawrence, Kansas 66045*
[12] *Luther College, Decorah, Iowa 52101*
[13] *University of Minnesota, Minneapolis, Minnesota 55455*
[14] *Northwestern University, Evanston, Illinois 60208*
[15] *State University of New York at Albany, Albany, New York 12222*

[16]*University of Oklahoma, Norman, Oklahoma 73019*
[17]*University of Pittsburgh, Pittsburgh, Pennsylvania 15260*
[18]*University of Puerto Rico, Mayaguez, Puerto Rico 00681*
[19]*Purdue University, West Lafayette, Indiana 47907*
[20]*Rensselaer Polytechnic Institute, Troy, New York 12180*
[21]*University of Rochester, Rochester, New York 14627*
[22]*Southern Methodist University, Dallas, Texas 75275*

(Dated: June 7, 2005)

Abstract

Using data accumulated with the CLEO-c detector on the $\psi(3770)$ resonance corresponding to a total integrated luminosity of 281 pb^{-1}, we measure the inclusive branching fractions of $D \to \eta X$, $D \to \eta' X$, and $D \to \phi X$, for both neutral and charged D mesons. The inclusive branching ratios for D^o are $(9.4 \pm 0.4 \pm 0.6)\%$, $(2.6 \pm 0.2 \pm 0.2)\%$ and $(1.0 \pm 0.1 \pm 0.1)\%$, for η, η' and ϕ, respectively, while for D^+ the rates are $(5.7 \pm 0.5 \pm 0.5)\%$, $(1.0 \pm 0.2 \pm 0.1)\%$ and $(1.1 \pm 0.1 \pm 0.2)\%$.

*Submitted to the XXII International Symposium on Lepton and Photon Interactions at High Energies, June 30-July 5, 2005, Uppsala, Sweden

I. INTRODUCTION

We report here on measurements of inclusive decays of η, η' and ϕ mesons from D^o and D^+ decays. These rates are interesting because they can be used when analyzing B^o, B^- and B_s meson decays. For example, properties of the B_s produced at the $\Upsilon(5S)$ resonance can be unraveled knowing these rates and the same ones from the D_s^+ [1].

The CLEO-c detector is equipped to measure the momenta and direction of charged particles, identify charged hadrons, detect photons, and determine with good precision their directions and energies. It has been described in more detail previously [2–5].

II. DATA SAMPLE AND SIGNAL SELECTION

In this analysis we use 281 pb^{-1} integrated luminosity of CLEO-c data produced in e^+e^- collisions and recorded at the ψ'' resonance (3.770 GeV). At this energy, the events consist of a mixture of pure D^+D^-, $D^o\overline{D}^o$, three-flavor continuum event and $\gamma\psi'$ events. There may also be small amounts of $\tau^+\tau^-$ pairs and two-photon events.

In this study we select events containing at least one charged or neutral D candidate in the modes listed in Table I. We use this sample to look for cases where we have $\eta \to \gamma\gamma$, $\eta' \to \pi^+\pi^-\eta$, $\eta \to \gamma\gamma$, or $\phi \to K^+K^-$ decays.

Particle identification, track, π^o and K_S selection criteria to reconstruct the D tags are identical to those described in reference [2] while the criteria for selecting η, η' and ϕ signals are described in detail in what follows.

III. RECONSTRUCTION OF D TAGGING MODES

Tagging modes are fully reconstructed by first evaluating the difference in the energy, ΔE, of the decay products with the beam energy. We require the absolute value of this difference to contain 98.8% of the signal events, i. e. to be within ~2.5 times the r.m.s width of the peak value. For final states consisting entirely of tracks, the ΔE resolution is $\sim$ 7 MeV. A π^o in the final state degrades this resolution by roughly a factor of two.

For the selected events we then view the reconstructed D beam-constrained mass defined as

$$m_{BC} = \sqrt{E_{beam}^2 - (\sum_i \overrightarrow{p}_i)^2}, \tag{1}$$

where i runs over all the final state particles. The beam-constrained mass has better resolution then merely calculating the invariant mass of the decay products since the beam has a small energy spread. We also use charge-conjugate tags; in the rest of this paper we will not mention the charge-conjugate modes explicitly, but they are always used.

The m_{BC} distributions for all $\overline{D^o}$ and D^- tagging modes considered in this data sample are shown in Fig. 1 and Fig. 2 respectively, and listed in Table I along with the numbers of signal events and background events within the signal region defined as containing 98.8% of the signal events with m_{BC} below the peak and 95.5% of the signal events above the peak; the interval varies from mode to mode. The event numbers are determined from fits of the m_{BC} distributions to a signal function plus a background shape. For the background we fit with a shape function analogous to one first used by the ARGUS collaboration [6] which has approximately the correct threshold behavior at large m_{BC} except for $\overline{D^o} \rightarrow K^-\pi^+$ and $\overline{D^o} \rightarrow K^-\pi^+\pi^o$ modes where we used a fourth order polynomial. To use both of these functions, we first fit it to the data selected by using 2.5 r.m.s. widths in the sideband region of the ΔE distribution of each mode, to fix the shape parameters in each mode allowing the normalization to float. For most of the modes, the signal is described by a Crystal Ball Line shape [7], a lineshape similar to that used for extracting photon signals from electromagnetic calorimeters because of the tail towards high m_{BC} caused by initial state radiation. The functional form is

$$f(m_{BC}|m_D, \sigma_{m_{BC}}, \alpha, n) = \begin{cases} A \cdot \exp\left[-\frac{1}{2}\left(\frac{m_{BC}-m_D}{\sigma_{m_{BC}}}\right)^2\right] & \text{for } m_{BC} < m_D - \alpha \cdot \sigma_{m_{BC}} \\ A \cdot \frac{\left(\frac{n}{\alpha}\right)^n e^{-\frac{1}{2}\alpha^2}}{\left(\frac{m_{BC}-m_D}{\sigma_{m_{BC}}}+\frac{n}{\alpha}-\alpha\right)^n} & \text{for } m_{BC} > m_D - \alpha \cdot \sigma_{m_{BC}} \\ \text{here } A^{-1} \equiv \sigma_{m_{BC}} \cdot \left[\frac{n}{\alpha} \cdot \frac{1}{n-1} e^{-\frac{1}{2}\alpha^2} + \sqrt{\frac{\pi}{2}}\left(1 + \text{erf}\left(\frac{\alpha}{\sqrt{2}}\right)\right)\right] \end{cases} \tag{2}$$

Here m_{BC} is the measured mass, m_D is the "true" (or most likely) mass and $\sigma_{m_{BC}}$ is the mass resolution. For the $\overline{D^o} \rightarrow K^-\pi^+\pi^o$ we add a Gaussian signal function to adequately fit the tails.

Tag	Mode	Signal	Background
	$K^+\pi^-\pi^-$	77387 ± 281	1868
	$K^+\pi^-\pi^-\pi^o$	24850 ± 214	12825
D^-	$K_s\pi^-$	11162 ± 136	514
	$K_s\pi^-\pi^-\pi^+$	18176 ± 255	8976
	$K_s\pi^-\pi^o$	20244 ± 170	5223
	Sum	151819 ± 487	29406
	$K^+\pi^-$	49418 ± 246	630
$\overline{D^o}$	$K^+\pi^-\pi^o$	101960 ± 476	18307
	$K^+\pi^-\pi^+\pi^-$	76178 ± 306	6421
	Sum	227556 ± 617	25357

TABLE I: Tagging modes and numbers of signal and background events determined from the fits shown in Fig. 1 and Fig. 2, and after making the mode dependant ΔE and beam constrained mass cuts.

We find $151819 \pm 487 \pm 455$ D^- and $227556 \pm 617 \pm 683$ $\overline{D^o}$ signal events that we use for further analysis. The systematic error on this number is given by varying the fitting functions and is estimated at 0.3%.

IV. SIGNAL SELECTION

We use the decay modes $\eta \rightarrow \gamma\gamma$, $\eta' \rightarrow \pi^+\pi^-\eta$, with the η subsequently decaying into $\gamma\gamma$ and $\phi \rightarrow K^+K^-$.

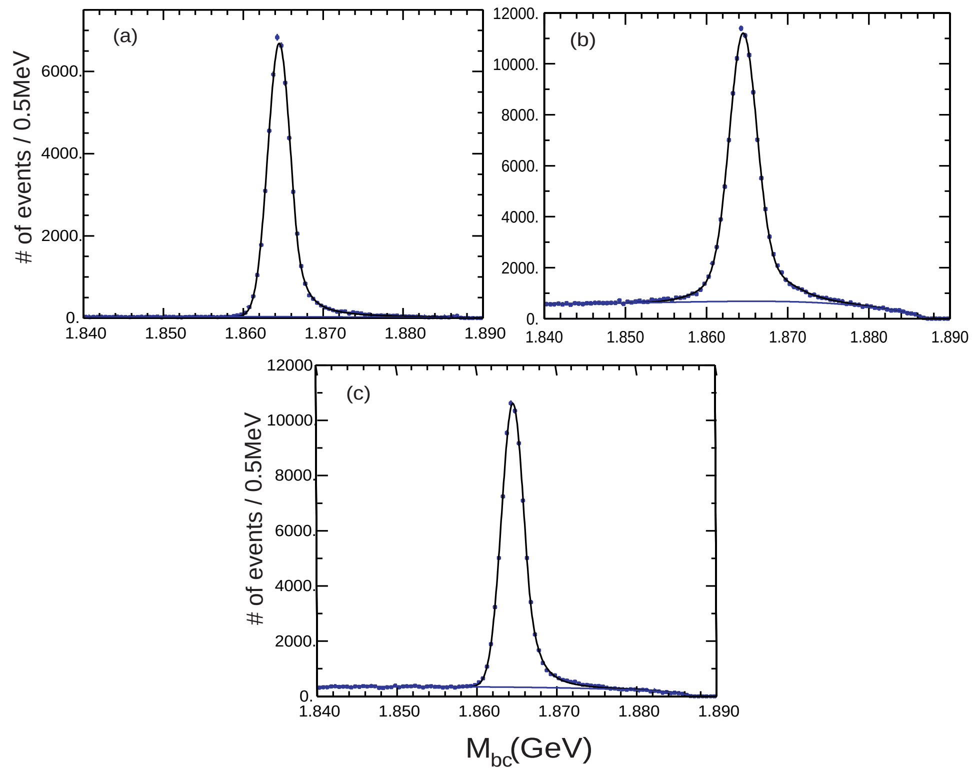

FIG. 1: Beam-constrained mass distributions for the fully reconstructed $\overline{D^o}$ decay candidates in the final states: (a) $K^+\pi^-$, (b) $K^+\pi^-\pi^o$, and (c) $K^+\pi^-\pi^-\pi^+$. The distributions are fit to a Crystal Ball Line shape for the signal. For the background, we either use a fourth order polynomial (in (a) and (b)) or an Argus shape (in (c)). Both background shapes are obtained from the ΔE sidebands.

For charged track candidates we insist that the distance of closest approach to the interaction vertex in the bending plane is less than 0.005 m and the distance of closest approach to the interaction vertex in the non-bending plane to be smaller than 0.05 m.

We distinguish between K and π candidates using dE/dx and RICH information that depend on track momenta. We define

$$PID_{dE/dx} = \sigma^2_{dE/dx,\pi} - \sigma^2_{dE/dx,K} \ , \tag{3}$$

$$PID_{RICH} = -2(lnL_\pi - lnL_K) \ , \tag{4}$$

where $\sigma_{dE/dx,i}$ is the difference between the measured dE/dx in the main Drift Chamber and the expected dE/dx value for a specific track (i), divided by the error in the dE/dx determination while L_i is the Likelihood of the particle, given by the measured Cherenkov angles of photons in the RICH detector compared with the predicted Cherenkov angles for that particular particle type (whenever RICH information is available, we require the existence of more than three Cherenkov photons).

For momenta higher than 0.7 GeV/c, we require:

- If dE/dx and RICH are both available:

  Cut on 3 $\sigma_{dE/dx,i}$ (dE/dx consistency cut),

  $(PID_{RICH} + PID_{dE/dx}) < 0$ for π's and $(PID_{RICH} + PID_{dE/dx}) > 0$ for K's.

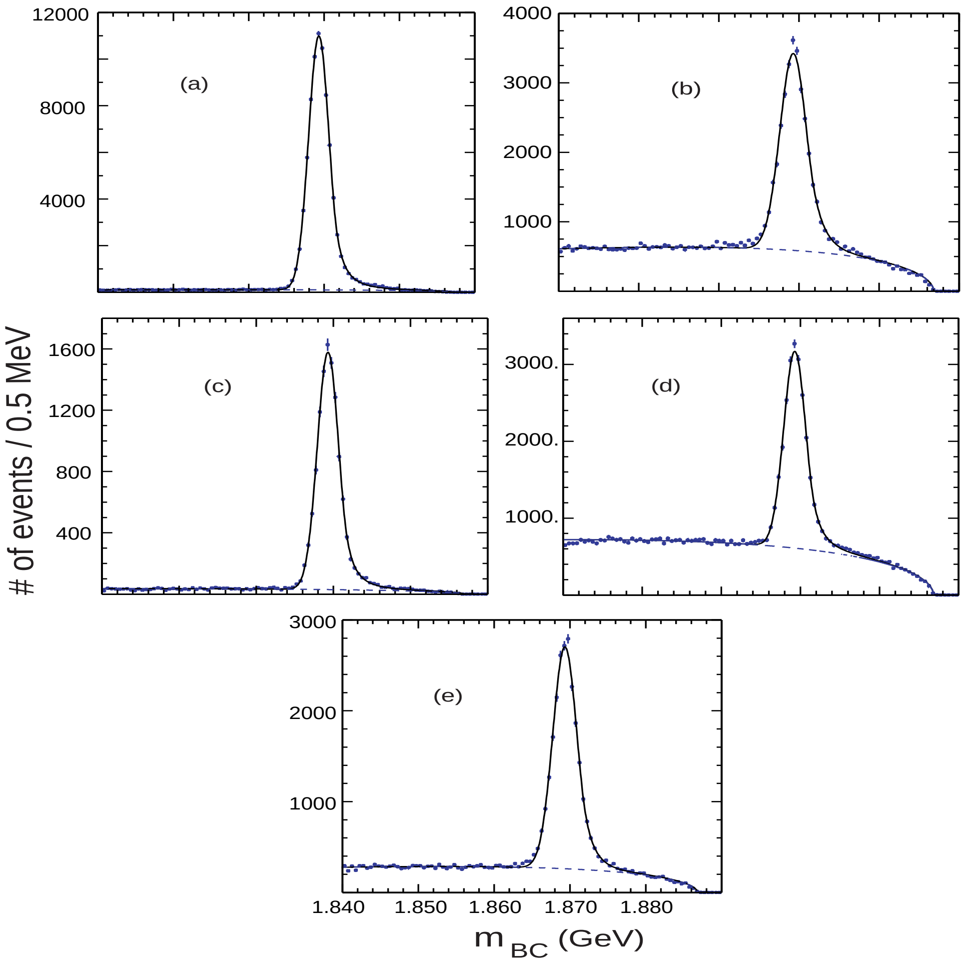

FIG. 2: Beam-constrained mass distributions for the fully reconstructed D^- decay candidates in the final states: (a) $K^+\pi^-\pi^-$, (b) $K^+\pi^-\pi^-\pi^o$, (c) $K_s\pi^-$, (d) $K_s\pi^-\pi^+\pi^-$, and (e) $K_s\pi^-\pi^o$. The distributions are fit to a Crystal Ball Line shape for the signal and an Argus shape obtained from the ΔE sidebands for the background.

- If RICH is available and dE/dx is not:

  $PID_{RICH} < 0$ for π's and $PID_{RICH} > 0$ for K's.

- If dE/dx is available and RICH is not:

  Cut on 3 $\sigma_{dE/dx,i}$

- If dE/dx and RICH are unavailable, use the track.

For momenta less than 0.7 GeV/c and higher than 0.2 GeV/c, we require:

- $PID_{dE/dx} < 0$ for pions and $PID_{dE/dx} > 0$ for kaons.
- Cut on 3 $\sigma_{dE/dx,i}$

For momenta less than 0.2 GeV/c, we loosen the dE/dx consistency requirement to 4 $\sigma_{dE/dx,i}$. For these two last cases (momentum less than 0.7 GeV/c), we accept the track if dE/dx is not available.

A. η, η' and ϕ Selection

We accept photons only in the good barrel region, $|\cos\theta| < 0.8$, where θ is the angle of the photon with respect to the beam direction. Photon candidates must not be matched to charged tracks, must have a reconstructed energy greater than 30 MeV and have a spatial distribution in the crystals consistent with that of an electromagnetic shower. In addition we require that the absolute value of cosine the angle between one of the photons and the η direction in the η rest-frame to be less than 0.85.

Candidates for η' mesons are selected using η candidates within 3 r.m.s. widths of the η mass and combining with a π^+ and a π^-. We then examine the mass difference between $\eta\pi^+\pi^-$ and η.

Candidates for ϕ mesons are formed from two oppositely charged kaon tracks. Both pions forming η' and kaons forming ϕ candidates are required to pass the track selection and particle identification requirements listed above.

V. BRANCHING RATIOS

A. Reconstruction Efficiencies

The reconstruction efficiencies for η, η' and ϕ in our tag samples of D^o and D^+ events, separately are shown in Fig. 3. They are determined from a Monte Carlo simulation of the detector.

Since our aim here is to measure the inclusive branching fractions, we break the η sample into two parts, one below 300 MeV/c and an other above, since the efficiency is constant at this point and higher.

For the η', the efficiency is constant with momentum, so we do not separate into momentum intervals. The ϕ efficiency, on the other hand, changes drastically with momentum and therefore we use several momentum regions. The increase in the ϕ efficiency is understood however from the fact that as the ϕ becomes more energetic, it becomes less probable that it is formed of a slow kaon (with momentum below 0.2 GeV/c).

B. Signal Yields

In order to evaluate the number of particles accruing in our signal sample due to the background events present in our single tag, we select another sample of events from 2.5 r.m.s. widths in the sideband region of the ΔE distributions. The sidebands are normalized to have the same number of events as the background under the peak and they are then subtracted to extract the yields.

In Fig. 4 and 5 we show the two-photon invariant mass in our two momentum intervals for both signal and sideband regions for D^o and D^+ tags respectively.

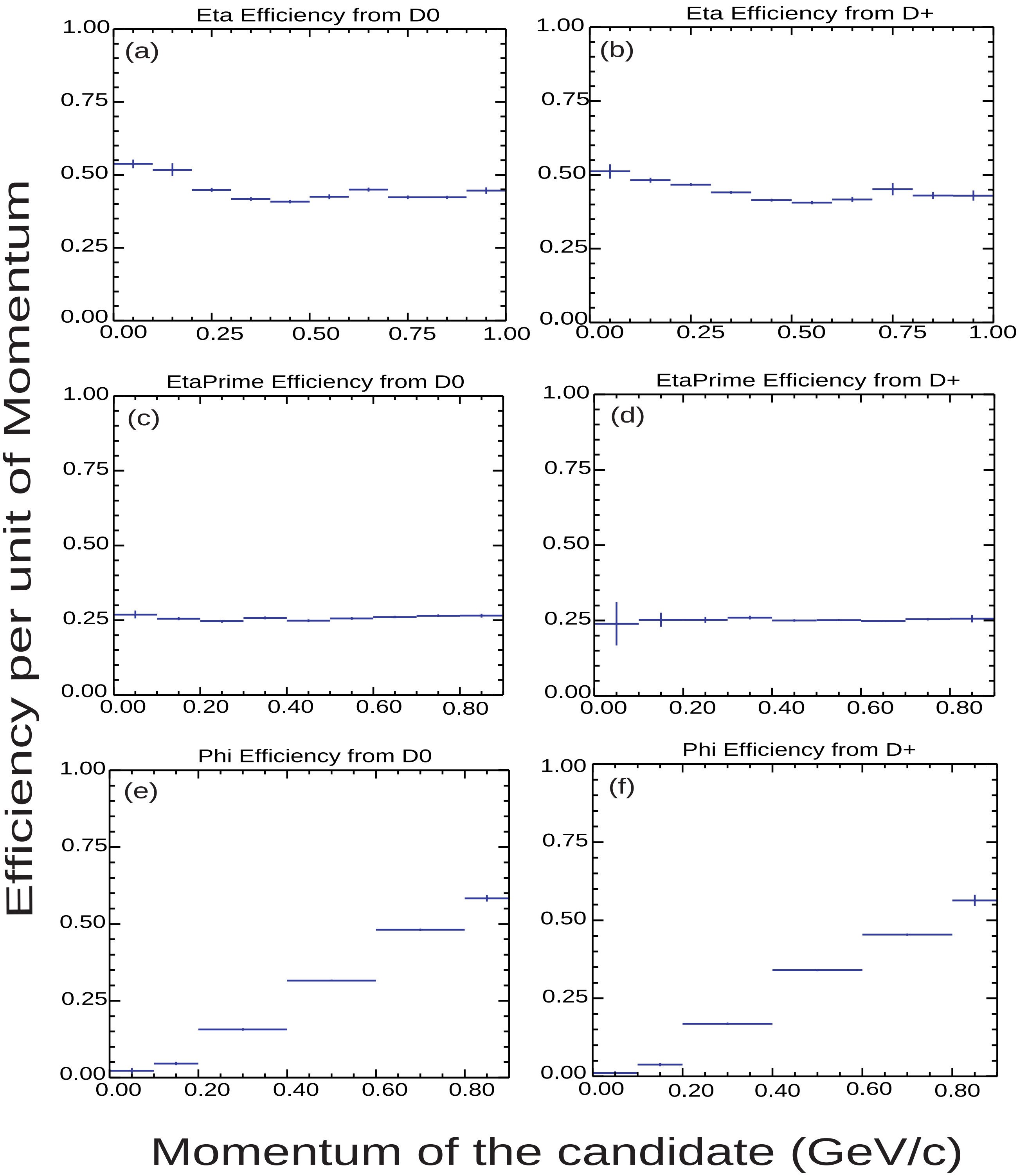

FIG. 3: Reconstruction efficiency of: (a) $\eta \to \gamma\gamma$ from $D^o\overline{D^o}$ events, (b) $\eta \to \gamma\gamma$ from D^+D^- events, (c) $\eta' \to \eta\pi^+\pi^-$ ($\eta \to \gamma\gamma$) from $D^o\overline{D^o}$ events, (d) $\eta' \to \eta\pi^+\pi^-$ ($\eta \to \gamma\gamma$) from D^+D^- events, (e) $\phi \to K^+K^-$ from $D^o\overline{D^o}$ events, (f) $\phi \to K^+K^-$ from D^+D^- events.

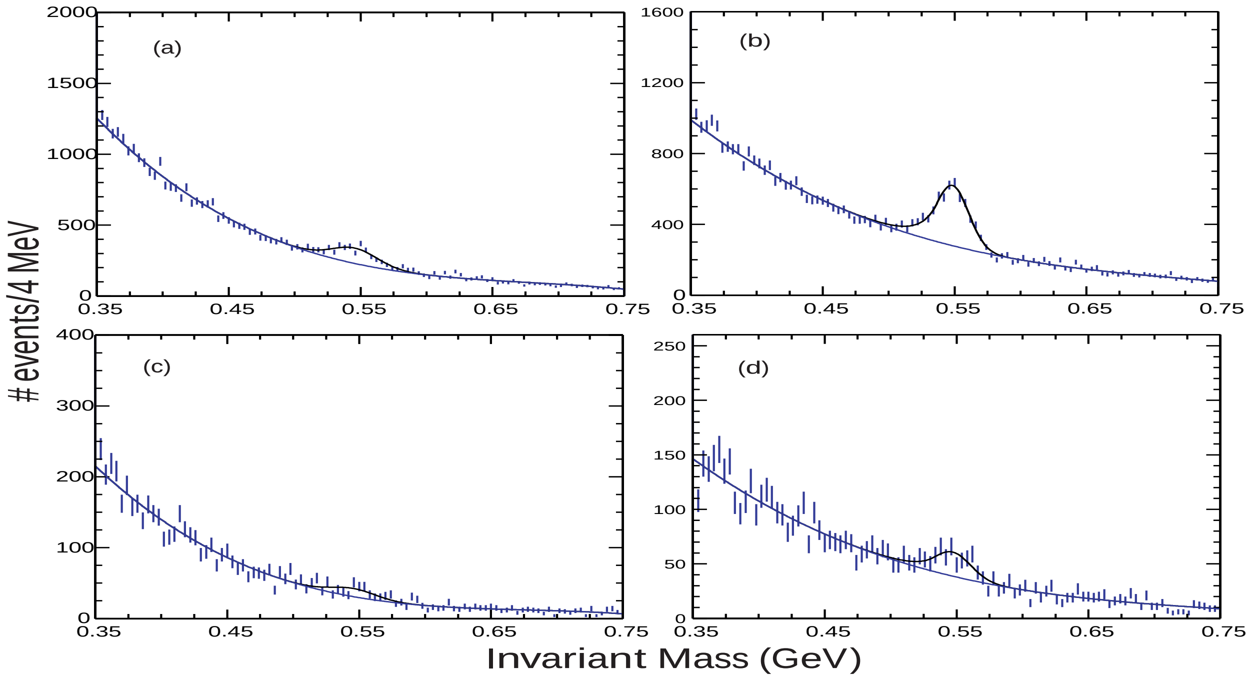

FIG. 4: Invariant mass of the $\eta \to \gamma\gamma$ candidates from $D^o\overline{D}^o$: (a) signal events with the momentum of η, $|p_\eta|$, less than 0.3 GeV/c, (b) signal events with $0.3 < |p_\eta| < 1.0$ GeV/c, (c) background events with $|p_\eta| < 0.3$ GeV/c, (d) background events with $0.3 < |p_\eta| < 1.0$ GeV/c.

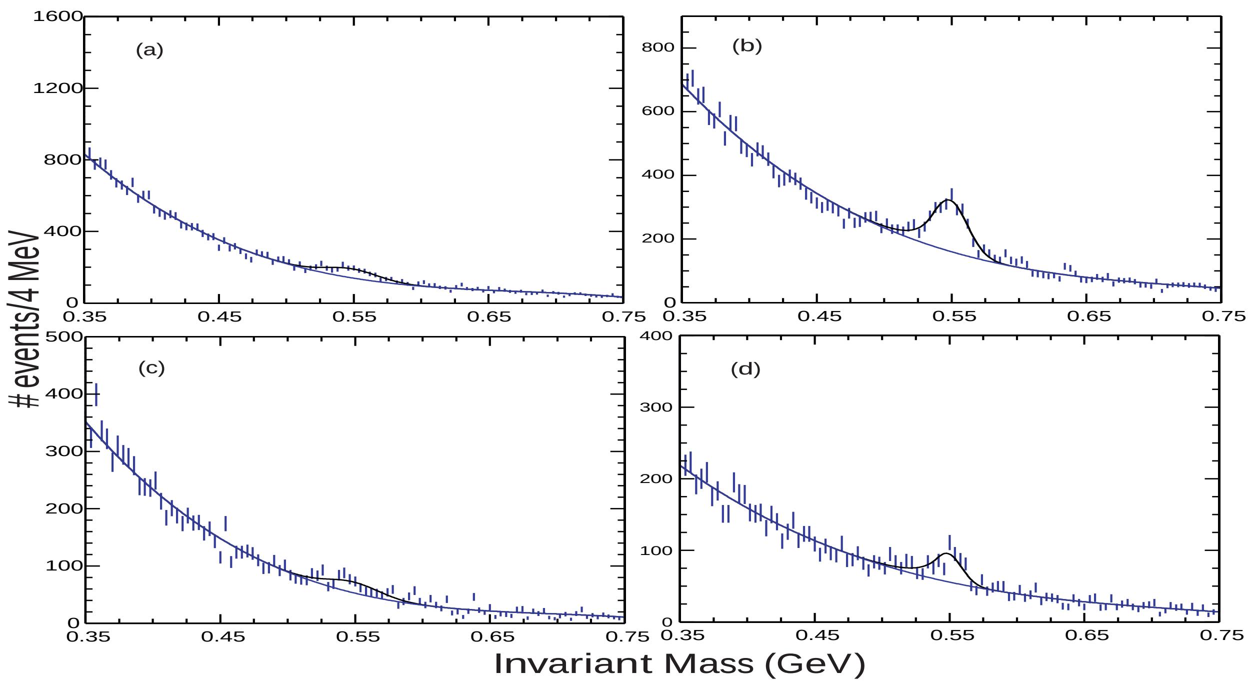

FIG. 5: Invariant mass of the $\eta \to \gamma\gamma$ candidates from D^+D^-: (a) signal events with the momentum of η, $|p_\eta|$, less than 0.3 GeV/c, (b) signal events with $0.3 < |p_\eta| < 1.0$ GeV/c, (c) background events with $|p_\eta| < 0.3$ GeV/c, (d) background events with $0.3 < |p_\eta| < 1.0$ GeV/c.

The η yields are determined by fits to a Crystal Ball function, to account for the low mass tail and a background polynomial. The signal, background and background subtracted yields, the detection efficiency and the branching fraction in each momentum interval are given in Table II. The inclusive branching ratios are hence $\mathcal{B}(D^o \to \eta X) = (9.4 \pm 0.4)\%$ and $\mathcal{B}(D^+ \to \eta X) = (5.7 \pm 0.5)\%$. The error is statistical only. Systematic errors will be discussed later.

Tag	$\|p_\eta\|$ (GeV/c)	N_η^{sig}	N_η^{bkg}	N_η	ϵ^i	$\mathcal{B}^i(D \to \eta X)$ (%)
D^o	0.0-0.3	1180.0 ± 108.2	125.5 ± 28.3	1054.5 ± 111.8	50.1	2.3 ± 0.2
	0.3-1.0	2889.9 ± 113.1	207.4 ± 40.4	2682.5 ± 120.1	42.4	7.0 ± 0.3
D^o(Total)	0.0-1.0	4069.9 ± 156.5	332.9 ± 49.3	3737.0 ± 164.1	–	9.4 ± 0.4
D^+	0.0-0.3	631.0 ± 98.9	234.7 ± 40.3	396.3 ± 106.8	48.7	1.4 ± 0.4
	0.3-1.0	1405.3 ± 88.0	299.3 ± 47.4	1106.0 ± 100.0	42.3	4.3 ± 0.4
D^+(Total)	0.0-1.0	2036.3 ± 132.4	534.0 ± 62.2	1502.3 ± 146.3	–	5.7 ± 0.5

TABLE II: η signal yields (N_η^{sig}), background yields (N_η^{bkg}) and background subtracted yields (N_η) vs momentum from D^o and D^+ events. Also listed are the η reconstruction efficiencies (ϵ^i), and the partial $D^o \to \eta X$ and $D^+ \to \eta X$ branching fractions vs momentum.

In Fig. 6 we show the $\eta\pi^+\pi^-$ - η mass difference for D^o and D^+ tags respectively from both signal and sideband regions. To determine the yields in this case we fit to a Gaussian signal function and a background polynomial. The signal, background, and background subtracted yields, the detection efficiency and the branching fraction in each momentum interval are given in Table III. The inclusive branching ratios are $\mathcal{B}(D^o \to \eta' X) = (2.6 \pm 0.2)\%$ and $\mathcal{B}(D^+ \to \eta' X) = (1.0 \pm 0.2)\%$, where the error is statistical only.

Tag	$N_{\eta'}^{sig}$	$N_{\eta'}^{bkg}$	$N_{\eta'}$	ϵ^i	$\mathcal{B}^i(D \to \eta' X)(\%)$
D^o	279.6 ± 19.0	12.4 ± 5.0	267.2 ± 19.6	25.7	2.6 ± 0.2
D^+	73.5 ± 11.7	4.5 ± 4.9	68.9 ± 12.6	25.1	1.0 ± 0.2

TABLE III: η' signal yields ($N_{\eta'}^{sig}$), background yields ($N_{\eta'}^{bkg}$) and background subtracted yields ($N_{\eta'}$) vs momentum from D^o and D^+ events. Also listed are the η' reconstruction efficiencies (ϵ^i), and the partial $D^o \to \eta' X$ and $D^+ \to \eta' X$ branching fractions vs momentum.

In Fig. 7, 8, 9 and 10 we show the K^+K^- invariant mass in five different momentum intervals from both signal and sideband regions for D^o and D^+ tags respectively. The signals are fit with a sum of two Gaussian shapes and the background is fit to a polynomial. The signal, background, and background subtracted yields, the detection efficiency and the branching fraction in each momentum interval from D^o and D^+ are given in Table IV and Table V respectively. The inclusive branching ratios are $\mathcal{B}(D^o \to \phi X) = (1.0 \pm 0.1)\%$ and $\mathcal{B}(D^+ \to \phi X) = (1.1 \pm 0.1)\%$, where the error is statistical only.

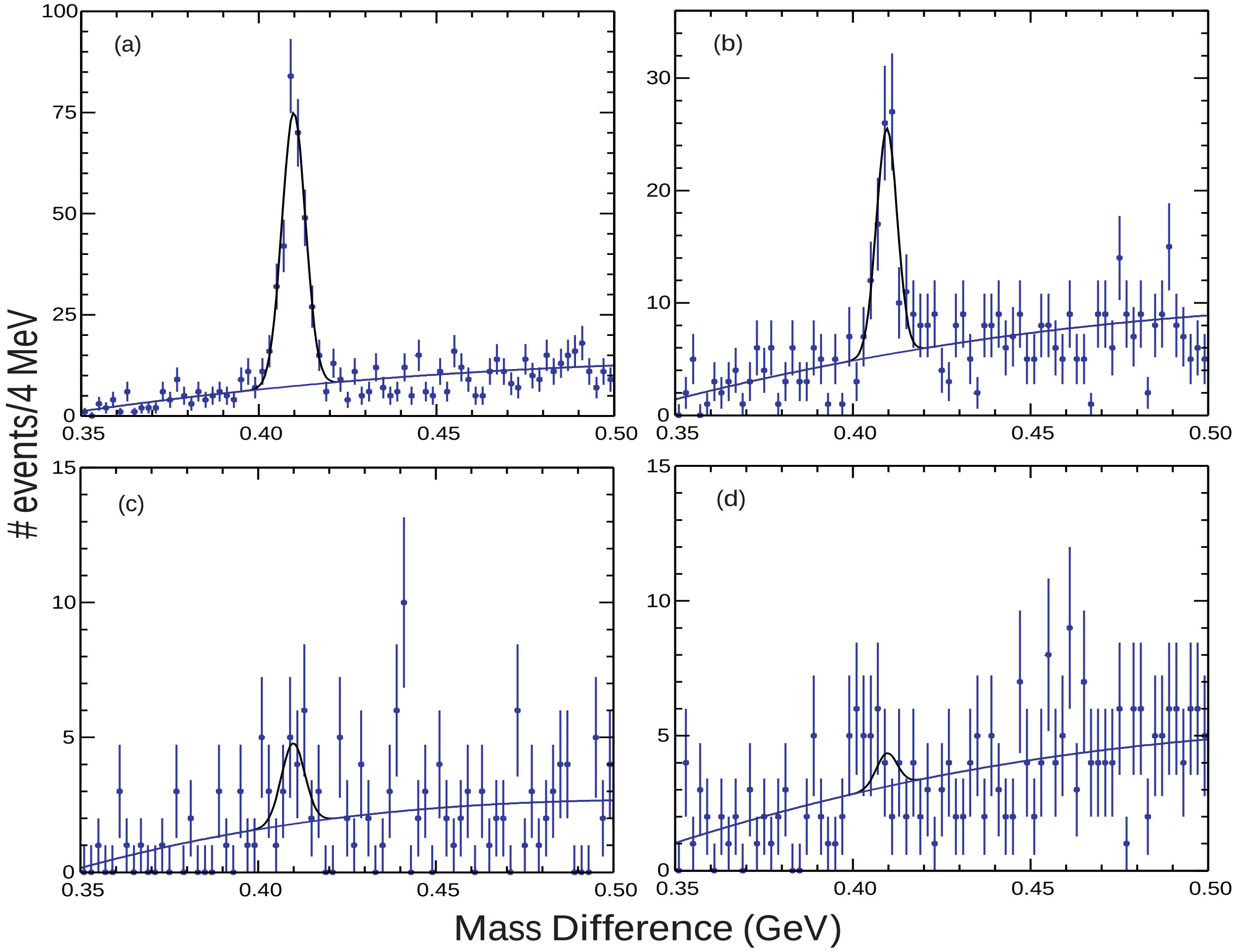

FIG. 6: Difference in the invariant mass of $\eta' \to \eta\pi^+\pi^-$ and η ($\eta \to \gamma\gamma$) candidates from: (a) $D^o\overline{D}^o$ signal events (b) D^+D^- signal events (c) $D^o\overline{D}^o$ background events, and (d) D^+D^- background events.

$\lvert p_\phi \rvert$ GeV/c	N_ϕ^{sig}	N_ϕ^{bkg}	N_ϕ	ϵ^i	$\mathcal{B}^i(D^+ \to \phi X)(\%)$
0.0 - 0.2	1.0 ± 1.0	1.0 ± 1.0	0.0 ± 0.8	3.4	0.00 ± 0.02
0.2 - 0.4	25.4 ± 6.7	2 ± 1.4	23.4 ± 6.8	15.6	0.13 ± 0.04
0.4 - 0.6	171.9 ± 18.1	3.9 ± 3.3	168.0 ± 18.4	31.2	0.48 ± 0.05
0.6 - 0.8	209.7 ± 17.6	10.2 ± 3.6	199.5 ± 18.0	48.1	0.37 ± 0.03
0.8 - 0.9	8.7 ± 3.5	1.0 ± 1.0	7.7 ± 3.7	58.3	0.01 ± 0.01
Total					
0.0 - 1.0	416.6 ± 26.4	18.0 ± 5.3	398.5 ± 26.9	–	1.0 ± 0.1

TABLE IV: ϕ signal yields (N_ϕ^{sig}), background yields (N_ϕ^{bkg}) and background subtracted yields (N_ϕ) vs momentum from D^o events. Also listed are the ϕ reconstruction efficiencies (ϵ^i), and the partial $D^o \to \phi X$ branching fractions vs momentum.

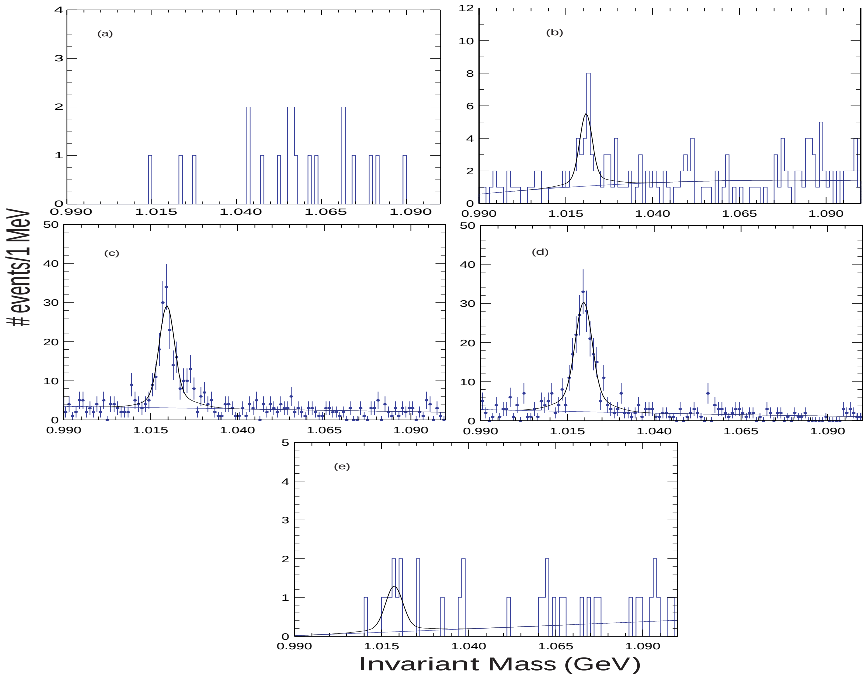

FIG. 7: Invariant mass of $\phi \to KK$ candidates from $D^o\overline{D}^o$ signal events in five different momentum intervals: (a) $0.0 < |p_\phi| < 0.2$ GeV/c, (b) $0.2 < |p_\phi| < 0.4$ GeV/c, (c) $0.4 < |p_\phi| < 0.6$ GeV/c, (d) $0.6 < |p_\phi| < 0.8$ GeV/c, (e) $0.8 < |p_\phi| < 0.9$ GeV/c.

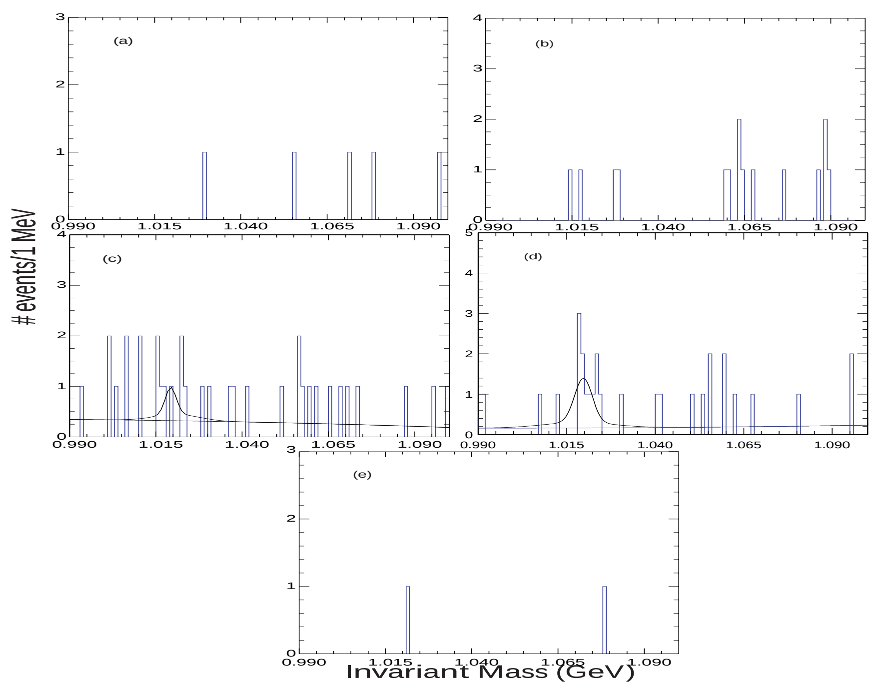

FIG. 8: Invariant mass of $\phi \to KK$ candidates from $D^o\overline{D}^o$ sideband events in five different momentum intervals: (a) $0.0 < |p_\phi| < 0.2$ GeV/c, (b) $0.2 < |p_\phi| < 0.4$ GeV/c, (c) $0.4 < |p_\phi| < 0.6$ GeV/c, (d) $0.6 < |p_\phi| < 0.8$ GeV/c, (e) $0.8 < |p_\phi| < 0.9$ GeV/c.

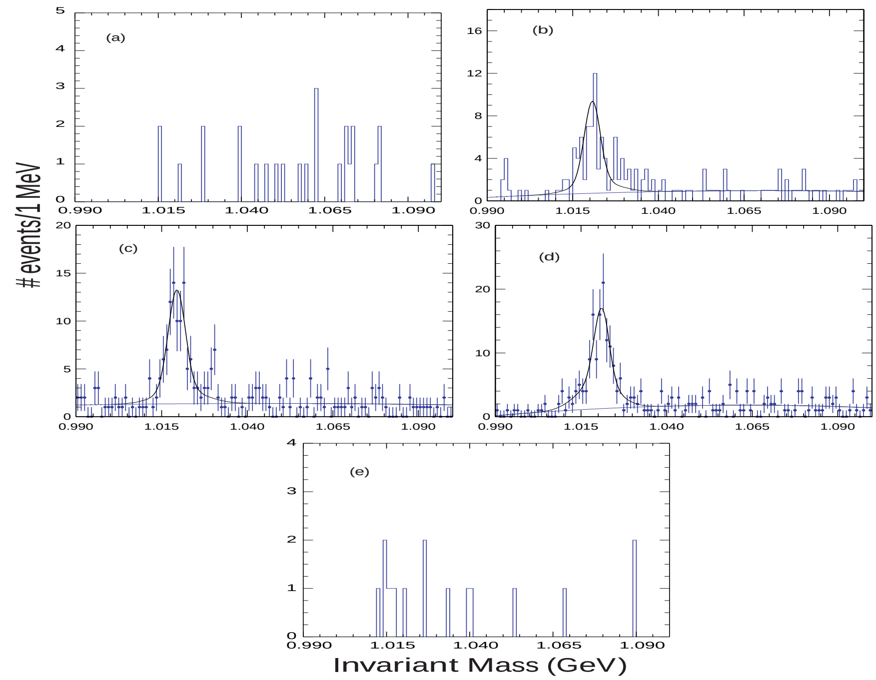

FIG. 9: Invariant mass of $\phi \rightarrow KK$ candidates from D^+D^- signal events in five different momentum intervals: (a) $0.0 < |p_\phi| < 0.2$ GeV/c, (b) $0.2 < |p_\phi| < 0.4$ GeV/c, (c) $0.4 < |p_\phi| < 0.6$ GeV/c, (d) $0.6 < |p_\phi| < 0.8$ GeV/c, (e) $0.8 < |p_\phi| < 0.9$ GeV/c.

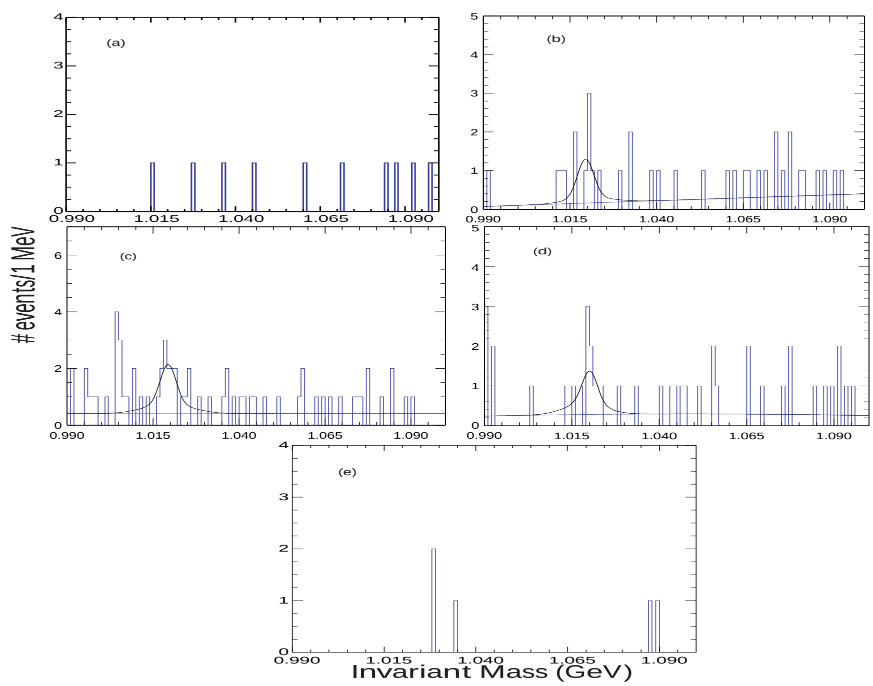

FIG. 10: Invariant mass of $\phi \rightarrow KK$ candidates from D^+D^- sideband events in five different ϕ momentum intervals: (a) $0.0 < |p_\phi| < 0.2$ GeV/c, (b) $0.2 < |p_\phi| < 0.4$ GeV/c, (c) $0.4 < |p_\phi| < 0.6$ GeV/c, (d) $0.6 < |p_\phi| < 0.8$ GeV/c, (e) $0.8 < |p_\phi| < 0.9$ GeV/c.

$\|p_\phi\|$ GeV/c	N_ϕ^{sig}	N_ϕ^{bkg}	N_ϕ	ϵ^i	$\mathcal{B}^i(D^+ \to \phi X)(\%)$
0.0 - 0.2	2.0 ± 1.4	1 ± 1	1.0 ± 1.7	2.4	0.06 ± 0.10
0.2 - 0.4	61.2 ± 9.7	8.1 ± 3.5	53.1 ± 10.3	16.8	0.42 ± 0.08
0.4 - 0.6	89.6 ± 12.2	12.5 ± 4.5	77.1 ± 13.0	34.0	0.30 ± 0.05
0.6 - 0.8	122.8 ± 12.5	8.5 ± 3.6	114.3 ± 13.0	45.4	0.34 ± 0.04
0.8 - 0.9	3.0 ± 1.7	3.0 ± 1.7	0.0 ± 0.8	56.3	0.000 ± 0.002
Total					
0.0 - 0.9	278.6 ± 20.1	33.0 ± 7.0	245.6 ± 21.3	–	1.1 ± 0.1

TABLE V: ϕ signal yields (N_ϕ^{sig}), background yields (N_ϕ^{bkg}) and background subtracted yields (N_ϕ) vs momentum from D^+ events. Also listed are the ϕ reconstruction efficiencies (ϵ^i), and the partial $D^+ \to \phi X$ branching fractions vs momentum.

VI. SYSTEMATIC UNCERTAINTIES

The systematic errors are dominated by the error on the number of particle yields and by simulation of the detection efficiency. For the η we estimate a detection efficiency error of $\pm 2\%$ per photon for a total of 4%. For the η' we have an additional 0.7% per track for track finding and fitting and 1% for particle identification for a total of 2.4% added in quadrature to the 4% for the η giving a systematic error on η' detection of 4.7%. Similarly, we estimate a systematic error on ϕ detection of 3.4% including both track finding (1.4% per kaon track candidate) and particle identification (1% per track). The efficiency errors contributions for η, η' and ϕ are listed in Table VI along with the total efficiency error for each particle.

To confirm the stability of the analysis, the measurements were redone with different set of tagging modes, different ΔE and beam constrained mass cuts. The results were consistent with our nominal values. Also we reconstructed the η, η' and ϕ from large statistics $D\overline{D}$ simulated events and were able to reproduce the input inclusive branching fractions.

	Systematic errors (%)
Pion track finding	0.7
Kaon track finding	1.4
PID cut	1.0
photon reconstruction	2
Number of tags	0.3
η Total	4.0
η' Total	4.7
ϕ Total	3.4

TABLE VI: Systematic errors on the $D^{0(+)} \to \eta, \eta', \phi X$ reconstruction efficiencies.

VII. CONCLUSIONS

Our results are summarized in Table VII. We are consistent with the PDG upper limits [8] where they exist and the one measurement for $D^o \to \phi X$, where our value is much more precise.

Mode	D^o(%)		D^+(%)	
	Our result	PDG	Our result	PDG
η X	9.4±0.4±0.6	<13	5.7±0.5±0.5	<13
η' X	2.6±0.2±0.2	-	1.0±0.2±0.1	-
ϕ X	1.0±0.1±0.1	1.7±0.8	1.1±0.1±0.2	<1.8

TABLE VII: Summary of inclusive branching ratio results.

These particles all have significant components of $s\bar{s}$. Our results show that η' and ϕ are relative rare in D^o and D^+ decay while the lighter η is produced at an almost order of magnitude higher rate. We expect that the η' and ϕ are produced at much higher rates in D_s decays. Summing over the known exclusive decays of the D_s gives inclusive yields of about 16% for each particle, with a rather large uncertainties. The large asymmetry between the yields of these particles between D_s and the lighter D mesons will allow us to probe B_s decays at the Υ(5S). Similar inclusive measurements of the D_s will make these studies even more useful.

VIII. ACKNOWLEDGMENTS

We gratefully acknowledge the effort of the CESR staff in providing us with excellent luminosity and running conditions. This work was supported by the National Science Foundation and the U.S. Department of Energy.

[1] D. Asner *et al.,* [CLEO Collaboration] ICHEP04-ABS11-0778 [arXiv:hep-ex/0408070], R. Sia [for CLEO collaboration] DPF 2004 [arXiv:hep-ex/0410087].

[2] G. Bonvicini *et al.* CLEO, Phys. Rev. **D70**, 112004 2004 [hep-ex/0411050].

[3] Y. Kubota *et al.* (CLEO), Nucl. Instrum. and Meth. **A320**, 66 (1992).

[4] D. Peterson *et al.*, Nucl. Instrum. and Meth. **A478**, 142 (2002).

[5] M. Artuso *et al.*, Nucl. Instrum. and Meth. **A502**, 91 (2003).

[6] The function is $f(m_{BC}) = A(m_{BC}+B)\sqrt{1-\left(\frac{m_{BC}+B}{C}\right)^2}\, e^{D\left(1-\left[\frac{m_{BC}+B}{C}\right]^2\right)}$. Here A is the overall normalization and B, C and D are parameters that govern the shape. See H. Albrecht *et al.* (ARGUS), Phys. Lett. B **229**, 304(1989).

[7] T. Skwarnicki, "A Study of the Radiative Cascade Transitions Between the Upsilon-Prime and Upsilon Resonances," DESY F31-86-02 (thesis, unpublished) (1986).

[8] S. Eidelman *et al.* (PDG), Phys. Lett. B **592**, 1 (2004).